

## A Synoptic Scale Perspective of Solar Forcing on Extreme Precipitation and Floods Over Europe During Summer

N. Rimbu<sup>1</sup> , T. Spiegl<sup>1</sup>, M. Ionita<sup>1,2</sup> , S. Doshi<sup>1</sup>, and G. Lohmann<sup>1,3</sup> 

<sup>1</sup>Alfred Wegener Institute Helmholtz Center for Polar and Marine Research, Section Paleoclimate Dynamics, Bremerhaven, Germany, <sup>2</sup>Faculty of Forestry, “Stefan cel Mare” University of Suceava, Suceava, Romania, <sup>3</sup>MARUM—Center for Marine Environmental Sciences, University of Bremen, Bremen, Germany

### Key Points:

- Low solar irradiance is associated with more frequent Rossby wave packets and extreme precipitation over western Europe during summer.
- Paleoclimate data suggests that these links are robust across different timescales.
- In the scenario of decreasing solar irradiance during next decades/centuries, an increase in Sun-related precipitation extremes is expected.

### Supporting Information:

Supporting Information may be found in the online version of this article.

### Correspondence to:

N. Rimbu,  
[Norel.Rimbu@awi.de](mailto:Norel.Rimbu@awi.de)

### Citation:

Rimbu, N., Spiegl, T., Ionita, M., Doshi, S., & Lohmann, G. (2024). A synoptic scale perspective of solar forcing on extreme precipitation and floods over Europe during summer. *Journal of Geophysical Research: Atmospheres*, 129, e2024JD041952. <https://doi.org/10.1029/2024JD041952>

Received 7 AUG 2024

Accepted 28 SEP 2024

**Abstract** The relationship between total solar irradiance (TSI) forcing and summer extreme precipitation and flood frequency over western Europe is investigated from a synoptic-scale perspective, with a focus on the role of Rossby wave packets (RWPs). Utilizing observational, model, and proxy data, we reveal a significant increase in RWP frequency along a zonal band centered around 50°N, extending from North America to western Europe, during periods of low TSI. This anomaly in RWP frequency is consistent with a significant increase in the frequency of extreme precipitation events recorded over western Europe. Sensitivity experiments conducted with a state-of-the-art chemistry-climate model corroborate our findings based on observational data. Additionally, a flood record from western Europe demonstrates a significant increase in flood frequency during low TSI years, a relationship that persists across timescales. We argue that the frequency patterns associated with TSI forcing presented in this study are robust and, therefore, valuable for estimating the frequency of extreme precipitation events over western Europe under various solar irradiance scenarios. Moreover, our findings indicate that the North Atlantic sector is more responsive to changes in solar forcing during the boreal summer than previously thought, with this effect manifesting primarily on synoptic timescales rather than the long-term climatological mean.

**Plain Language Summary** The total solar irradiance change has a significant impact on precipitation extremes over western Europe. Based on statistical analysis of observed and reconstructed data, we show that during low total solar irradiance years the frequency of extreme precipitation and floods over western Europe is significantly higher than the climatology due to more frequent synoptic-scale Rossby wave packet (RWP) events. Analysis of paleoclimate data reveals similar relationships between total solar irradiance forcing and RWP and extreme precipitation frequency for different timescales. We argue that the RWP patterns presented here are useful to estimate the evolution of extreme precipitation and floods over western Europe during the next decades/centuries under different solar irradiance scenarios.

## 1. Introduction

The fluctuations in solar irradiance modulate Earth's climate system, including atmospheric composition (e.g., middle atmosphere ozone), tropical convection, and cloud formation and related dynamical feedbacks (e.g., Gray et al., 2010). The imprints of the solar forcing in the terrestrial climate system are often investigated by analyzing long-term annual mean changes in meteorological variables (Jones & Mann, 2004; Lohmann et al., 2004), such as global mean temperature or precipitation. Furthermore, explanatory approaches for more complex transmission mechanisms, which involve feedbacks between solar spectral irradiance, ozone, and altered propagation conditions of planetary waves and resulting atmospheric dynamics, predominately focus on the boreal winter of the Northern Hemisphere (Kodera & Kuroda, 2002 (and thereafter)) and have recently been shown to be incompletely and possibly inadequately understood (Chiodo et al., 2019; T. C. Spiegl et al., 2023).

In this study, we aim to expand the investigation to encompass potential signals across the Northern Hemisphere. In doing so, we examine the possible influence of solar forcing on meteorological extreme events operating on timescales ranging from days to a few weeks and their significance for documented past summer weather patterns. It's worth noting the paradoxical tendency to emphasize winter seasons in solar-terrestrial research, despite historical evidence, such as the early Spörer (1420–1440) and later Maunder Minimum (1675–1715), indicating that harsh cold winters were followed by particularly cool and humid summers (Büntgen et al., 2011; Luterbacher et al., 2001) and associated crop failures in Europe (Camenish et al., 2016).

© 2024. The Author(s).

This is an open access article under the terms of the [Creative Commons Attribution License](https://creativecommons.org/licenses/by/4.0/), which permits use, distribution and reproduction in any medium, provided the original work is properly cited.

Here we focus on the boreal summer and present a synoptic-scale interpretation of paleoclimate data showing an anticorrelation between changes in summer flood frequency over western Europe and solar irradiance (e.g., Czymzik et al., 2016). Transient Rossby wave packets (RWPs), a relevant synoptic-scale atmospheric circulation pattern, are important because they occur as precursors to extreme weather events such as intense surface cyclones and extreme temperatures and precipitation (e.g., Wirth et al., 2018). From a climatological perspective, RWPs are initiated most frequently in the entrance region of the midlatitude storm tracks in the western North Pacific and the western North Atlantic. They propagate along the midlatitude waveguide, a region with strong potential vorticity gradients that reduce the meridional dispersion of atmospheric waves. The RWPs decay preferentially in the exit regions of the storm tracks over North America and the Eastern Atlantic/Europe, a process related to Rossby wave breaking (RWB) (Quinting & Vitart, 2019). A signature of RWB in the Atlantic–European region is the upper-level high potential vorticity southward intrusions, which are associated with extreme water vapor transport and precipitation over western Europe (e.g., de Vries, 2021). Therefore, understanding the changes of the RWP properties is important for understanding extreme weather and climate variability.

Variability in the properties of RWPs has been intensively investigated in recent studies. For example, Souders et al. (2014) used 300-hPa streamline following envelope of meridional wind and found no trend in the annual mean RWP activity volume between 1979 and 2010 both for the whole and different sectors of the Northern Hemisphere. Karami (2019) used 250 hPa envelope of meridional wind and reported no trend in any sector or season of the Northern Hemisphere between 1980 and 2013. A recent study (Fragkoulidis, 2022) reports important decadal variability and trends in the amplitude, phase and phase-speed of RWPs during the observational period. Furthermore, analysis of model simulation data under different scenarios of greenhouse gas emissions reveals significant trends in RWP frequency for the next decades until the year 2100 (Trevisiol et al., 2022). These changes in RWP characteristics should be also detected in the frequency of extreme weather and climate records, as RWPs and weather extremes are strongly linked (e.g., Wirth et al., 2018). Nevertheless, to our knowledge, there are no available studies about RWP variability from a paleoclimate perspective.

Both internal and external forcing is responsible for the changes in RWP characteristics as presented in the above-mentioned studies. It is well known that climate modes, such as the Arctic/North Atlantic Oscillation (AO/NAO) or El Niño–Southern Oscillation (ENSO), alter the large-scale mid latitude flow and, therefore, the waveguide where RWPs propagate. There is a strong connection between AO/NAO and the frequency of wave breaking (e.g., Strong & Magnusdottir, 2008) and atmospheric blocking (Riviere & Orlansky, 2007), two phenomena that are intimately related to RWPs (Altenhoff et al., 2008). Pérez et al. (2021) reported a strong impact of the southern annular mode (SAM) on long-lived RWPs in the Southern Hemisphere in two reanalysis data sets during the 1979 to 2020 period. Therefore, part of interannual and longer timescale variability in RWPs, as identified in observational data, could be related to different modes of climate variability. External forcing, such as solar irradiance changes, modulate atmospheric dynamics and local climate modes in the midlatitudes (e.g., Gray et al., 2010; Roy, 2018) and thus potentially the RWP properties. To our knowledge, the sensitivity of RWP frequency and related weather extremes in response to changes in the solar irradiance was not yet investigated. Thus, the main goal of this study is to isolate RWP frequency anomaly patterns associated with low solar irradiance in the North Atlantic region and their relationship with extreme precipitation and floods over western Europe during boreal summer, both for instrumental and pre-instrumental period.

Building upon recent work by Rimbu et al. (2021), which suggested a potential link between solar irradiance variability and extreme weather and climate events over Europe during the boreal summer over the last millennium, this study delves deeper into the underlying mechanisms. While Rimbu et al. (2021) established an out-of-phase relationship between flooding frequency in Western Europe (as evidenced by Bavarian lake sediments) and the solar cycle, we extend this analysis to a synoptic scale. Specifically, we demonstrate that the observed increase in heavy precipitation days and floods over western Europe during periods of low solar irradiance is associated with an increased frequency of RWPs in the Atlantic–European region. Through the analysis of proxy data, we establish that the relationship between low solar irradiance forcing and increased frequency of extreme precipitation and floods over western Europe during boreal summer is consistent across the investigated time periods. Furthermore, we utilize explicitly designed model experiments to corroborate our findings based on proxy data and reanalysis.

Our study can serve as motivation for further in-depth investigations into the modulation potential of solar-driven extreme events during summer seasons in a future hothouse state. This is particularly relevant given that the

current evolution of various features of the Sun's magnetic field suggests an end to the current grand solar maximum period and a potential return of a modern grand solar minimum within the next decades. This could entail spatio-temporal solar-induced consequences projected onto anthropogenic climate change (e.g., Spiegl & Langematz, 2020). The availability of respective future solar scenarios to be included as part of CMIP6 (Matthes et al., 2017) or CMIP7 (Funke et al., 2024) underlines the relevance of the topic once more.

The paper is organized as follows. Section 2 describes the data, the algorithm to calculate RWP frequency, the analysis applied in this study, as well as the model design and experimental setup. Section 3 focuses on the solar irradiance impact on RWP and extreme precipitation frequency during the observational period. In the subsequent Section 4 we discuss the model results. The robustness of the RWPs and extreme precipitation frequency anomaly patterns, as derived from observational data, in a paleoclimate context is addressed in Section 5. Lastly, Section 6 provides a summary and discussion of the results.

## 2. Data and Methods

### 2.1. Total Solar Irradiance

The National Oceanic and Atmospheric Administration (NOAA) Climate Data Record (CDR) of Total Solar Irradiance (TSI), NRLTSI version 2.1 from the NOAA National Centers for Environmental Information for the period 1610–1849 with annual resolution (Coddington et al., 2017) has been used. The reconstruction model, which is an empirical one, takes into account that the balance between bright facular and dark sunspot features of the solar disk describe changes in solar irradiance from the background quiet-Sun conditions. The contribution of bright facular and dark sunspot are determined by linear regression between solar proxies and direct observations of TSI by satellite missions. This record was merged with the annual TSI record recommended for solar reference scenario CMIP6 model simulations, covering the period 1850–2299 (Matthes et al., 2017). The annual TSI time series for the period 1850–2299 was calculated from the available monthly mean time series. We used this record because its homogeneity in time, which is a necessary condition for a realistic solar forcing. The merged TSI time series cover the period 1610–2299 with annual resolution.

### 2.2. Rossby Wave Packets Frequency

The frequency of RWPs is calculated using the functions implemented in the R package metR (Campitelli, 2021), which are based on the algorithm described in Zimin et al. (2003). We chose this method because it is widely used (Quinting & Vitart, 2019; Trevisiol et al., 2022). Following Trevisiol et al. (2022) we estimate the Amplitude of the Wave Packet envelope (WPA) by considering 250 hPa meridional wind component ( $v$ ) to describe deviations from the zonal flow. A similar methodology was used by Karami (2019) to calculate WPA using NCEP reanalysis data. For each latitudinal circle of the N longitudinal points, the Fourier transform coefficients  $V_k$  of  $v$  have been calculated

$$V_k = \frac{1}{N} \sum_{l=1}^N v \left( \frac{2\pi l}{N} \right) e^{-\frac{2\pi i k l}{N}}, k = -\frac{N}{2} + 1, \dots, \frac{N}{2}$$

Then the signal has been reconstructed through the inverse Fourier transform for the wave numbers typical of synoptic scale, that is, 4 to 11 (e.g., Karami, 2019) as follows:

$$w \left( \frac{2\pi l}{N} \right) = 2 \sum_{k=4}^{k=11} V_k e^{\frac{2\pi i k l}{N}}$$

Finally, the WPA is estimated from the equation given below:

$$\text{WPA} \left( \frac{2\pi l}{N} \right) = \left| w \left( \frac{2\pi l}{N} \right) \right|$$

The WPA is estimated in each grid point, using the 250 hPa meridional wind retrieved from the NOAA-CIRES-DOE Twentieth Century Reanalysis Project, version 3, hereafter 20CRv3 (Slivinsky et al., 2019), database. The 250 hPa meridional wind for summer days, that is, from 1st June to 31st August (JJA), is used to calculate RWP

frequency. An RWP object is considered to be detected in a grid point if the WPA in that grid point is higher than 20 m/s. This threshold was used in previous studies (e.g., Karami, 2019; Trevisiol et al., 2022) to identify RWPs in the upper-level meridional wind field. The percentage of summer days for which an RWP event is detected, that is, WPA > 20 m/s, is calculated for each grid point for each summer using 250 hPa daily meridional wind retrieved from the 20CRv3 data set. The RWP frequency anomaly patterns associated with low total solar irradiance years are derived through a composite analysis. Furthermore we have used the daily Z500 field from the National Center for Environmental Prediction and National Center for Atmospheric Research (NCEP/NCAR) (hereafter NCEP) (e.g., Kalnay et al., 1996) as well as the Modern-Era Retrospective analysis for Research and Applications, version 2 (hereafter MERRA-2) (e.g., Gelaro et al., 2017) reanalysis databases to check the consistency of the RWP patterns associated with low TSI forcing.

### 2.3. Precipitation Extremes

Extreme precipitation events have been usually investigated using extreme indices recommended by the Expert Team on Climate Change Detection and Indices (ETCCDI) (Zhang et al., 2011). The ETCCDI is a set of internationally accepted indices based on daily air temperature and precipitation measures that elucidates changes in the frequency, duration and magnitude of extreme climate events. Here we use the R90p index, defined as the number of days in a summer with daily precipitation higher than the 90th percentile of precipitation of wet days ( $R > 1$  mm). This index is calculated in each grid-point for all summers covering the period 1806–2015 using 20CRv3 precipitation rate data.

### 2.4. Model Description and Experimental Setup

The sensitivity experiments analyzed have been conducted with ECHAM/MESSy in its version 2.52 (Jöckel et al., 2016). The model uses ECHAM5 (Roeckner et al., 2006) as a dynamical core and integrates the MECCA (Sander et al., 2005) interactive ozone chemistry in response to atmospheric tracers and solar spectral irradiance. The high-resolution short-wave radiation scheme, FUBRAD (Kunze et al., 2014; Nissen et al., 2007), extends upward from 70 hPa, encompassing the Lyman-alpha to the near-infrared spectrum across 81 wave length bands. With a vertical resolution of 47 levels, the model reaches a top altitude of 0.01 hPa. Spatially, the model operates at a horizontal resolution of T42 (approximately  $2.5^\circ \times 2.5^\circ$ ) and is coupled to MPIOM (Jungclaus et al., 2006), which operates at a resolution of approximately  $1.5^\circ \times 1.5^\circ$ .

To investigate the impact of a GSM-like downturn in solar input on RWP dynamics and meteorological extreme events in the summer season under preindustrial conditions, we analyzed a set of two distinct equilibrium simulations. The reference simulation (REF1850) represents steady-state conditions for greenhouse gases (GHGs) and ozone-depleting substances (ODSs) corresponding to the year 1850. The solar forcing applied in this reference experiment follows the 1850-PI scenario, as detailed by Matthes et al. (2017). The experiment under GSM conditions (GSM) uses the same settings (GHGs and ODSs) as REF1850 but assumes a severe Maunder Minimum-like downturn in solar energy. The GSM forcing includes a reduction of  $\sim -5.5$  W/m<sup>2</sup> in TSI and a respective adjustment of the SSI. The solar forcing data follow the PHI-MC17 scenario as discussed in Egorova et al. (2018). To account for Maunder Minimum conditions, TSI and SSI were averaged over the years 1690–1710, and the resulting values were then prescribed as constant. After both experiments reached equilibrium, 150 transient years were evaluated. These experiments were part of the SOLCHECK project. More details and data can be found in T. Spiegl et al. (2023).

### 2.5. Paleoclimate Data

To put the atmospheric circulation and precipitation extremes associated with low TSI, as derived from observational data, into a long-term perspective, we use paleoclimate data. The 500 hPa field (Z500), retrieved from Mode-RA paleo-reanalysis data base (Valler et al., 2023, 2024) is used to obtain the atmospheric circulation pattern associated with low TSI forcing during the 1610–2008 period. This period is covered by both TSI and Z500 records. The summer Z500 data, used in composite analysis, is calculated from the corresponding June, July and August Z500 fields. This reconstruction is based on an offline data assimilation approach, blending together information from an ensemble of transient atmospheric model simulations, observations and proxy data (Valler et al., 2024).

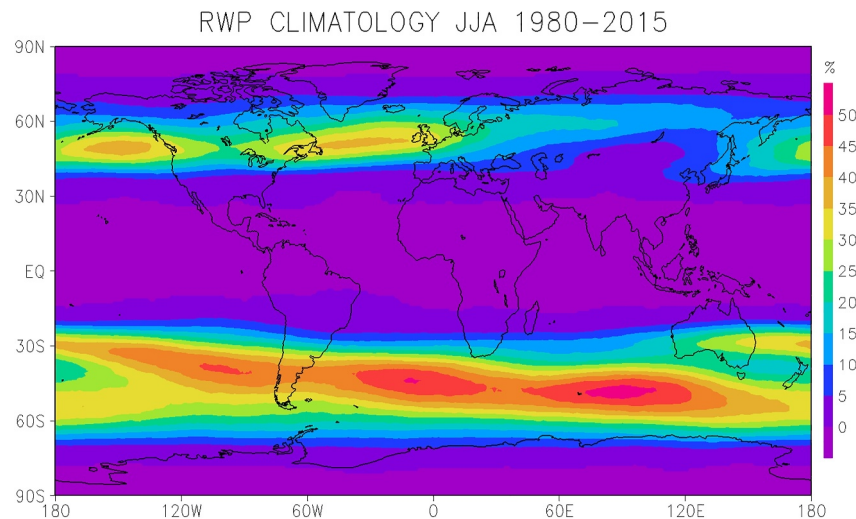


**Figure 1.** Summer climatology of relative frequency of WPAs exceeding 20 m/s for each grid point, processing 20CRv3 data set for 1980–2015 period. Units: percentage of days with WPA >20 m/s from total number of summer days.

Furthermore, the sediment record from the Lake Ammer, that is, Ammersee in German terminology (Czymzik et al., 2012), is used here to look for TSI-flood relationship during the past. The river Ammer rises in the Bavarian Alps and flows northward for about 80 km to Ammersee (48.01°N; 11.12°E). Details about river Ammer and its catchment can be found in Czymzik et al., 2012 (and references therein). High daily discharges of this river, that is, floods, are associated with specific layers in the lake sediments, which can be used to reconstruct flood frequency. Here we use the annual resolution flood frequency reconstruction going back to mid-Holocene (e.g., Czymzik et al., 2013). It was found that this record is a good proxy for heavy rainfall and flood frequency over western Europe (Rimbu et al., 2016, 2021). This record covers the period 3563 BC to 1999 AD with annual resolution (Czymzik et al., 2013).

## 2.6. Analysis Methods

Composite (threshold of  $-0.5$  sigma) is used to identify patterns of RWP and extreme precipitation indices for low TSI years. Note that TSI time series is linearly detrended and normalized with its standard deviation for the analysis period. Composite maps are constructed by averaging the RWP or R90p frequency anomalies over years corresponding to low total TSI values. Anomalies are calculated relative to the climatology of the analysed period. The significance of the composite anomalies and correlations are calculated at each grid point using a simple  $t$ -test (e.g., von Storch and Zwiers, 1999). As we focus on interannual to multidecadal timescales, both RWP and R90p fields are linearly detrended before the composite analysis.

## 3. Rossby Wave Packets and Extreme Precipitation Frequency Patterns Associated With Low Solar Irradiance Forcing During the Observational Period

As a first step the climatology of the summer RWP events, over the period 1980–2015, was analyzed to facilitate comparison with previously published RWP frequency climatologies (e.g., Karami, 2019; Trevisiol et al., 2022). This climatology reveals three prominent storm tracks, identified as regions of high RWP frequency: the North Atlantic (NA) storm track extending from the eastern North American coast to Europe; the North Pacific (NP) storm track extending from the Okhotsk Sea to the northwestern American coast; and the Southern Hemisphere (SH) storm track spreading around 50°S. A weaker storm track affecting the Russian area is also evident (Figure 1). The global RWP frequency pattern aligns with that presented by Karami (2019) based on NCEP data, although RWP frequencies in our climatology (Figure 1) are systematically lower. This discrepancy is likely attributable to differences in the spatial resolution of the underlying data products or other methodological variations. To further assess the robustness of our findings, RWP climatologies for extended periods were calculated using NCEP and MERRA-2 data (1948–2022 and 1980–2022, respectively) (Figure S1 in Supporting Information S1). These climatologies exhibit similar patterns to the 20CRv3 RWP climatology for 1980–2015

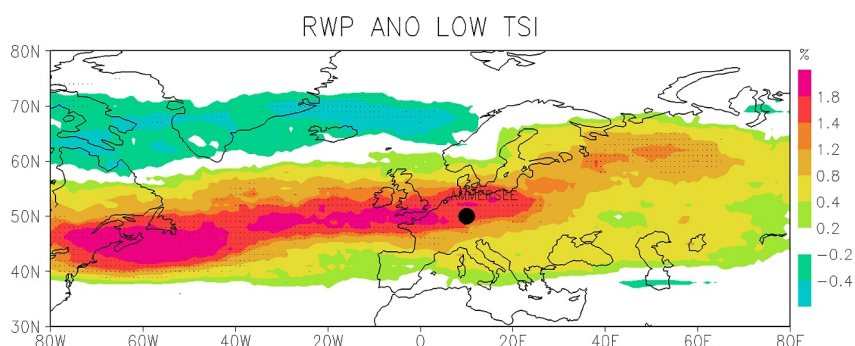


**Figure 2.** Composite map of the RWP frequency anomalies during summer for low total solar irradiance years during 1806–2015. The lake sediment location, that is, Ammersee, is indicated by the filled circle. The dots mark cells with significant changes (90% confidence level). Units: %.

(Figure 1). Our study focuses on the changes in RWP frequency, or storm track activity, in the Atlantic–European region in response to TSI forcing.

The composite map of this field (i.e., RWP) in relation to the total solar irradiance time series, shows a significant increase in the RWP frequency in a region extending from the eastern part of North America to the western part of Europe, along  $\sim 50^\circ\text{N}$ , for low solar irradiance years (Figure 2). North of the positive RWP anomalies, around  $\sim 65^\circ\text{N}$ , negative RWP frequency anomalies are recorded (Figure 2). As the RWPs form and propagate in the storm track region (e.g., Wirth et al., 2018), Figure 2 suggests a southward displacement of the NA storm track during low solar irradiance years. This finding aligns with previous modeling studies (e.g., Haigh, 1999) that have demonstrated a general poleward shift of Northern Hemisphere storm tracks under high TSI forcing. Notably, our lake sediment record (Figure 2, filled black circle) is situated within a region exhibiting positive anomalies in RWP frequency. Similar RWP frequency anomaly patterns associated with low TSI are observed for shorter periods, specifically 1980–2022 using MERRA-2 data (Figure S2a in Supporting Information S1) and 1948–2022 using NCEP data (Figure S2b in Supporting Information S1).

To better assess and confirm the anticorrelation between RWP frequency and TSI we define an index as the average RWP frequency within the region ( $80^\circ\text{W}$ – $20^\circ\text{E}$ ;  $45^\circ\text{N}$ – $55^\circ\text{N}$ ). In this region the RWP frequency anomalies, as shown on the RWP frequency composite map (Figure 2), are highly significant. There is a strong increasing trend in the RWP index based on 20CRv3 data during 1806–2015 period (Figure S3 in Supporting Information S1). As this trend is possibly related to a continuous increase in quantity and quality of observed data used in the 20CRv3 assimilation system, we removed the linear trend before any analysis. Furthermore, the values of this index calculated using NCEP as well as MERRA-2 data are systematically higher than those of the 20CRv3 index (Figure S3 in Supporting Information S1). Therefore, after removing linear trends, these time series were normalized with the corresponding standard deviation before any analysis. The resulting time series are highly ( $r > 0.65$ ) correlated over their common period. The linearly detrended and normalized 20CRv3 RWP index (Figure 3a) is significantly negatively correlated ( $r = -0.20$ ;  $p < 0.01$ ) with TSI over the 20CRv3 period, that is, 1806–2015. The RWP index for the period 1980–2022, calculated using MERRA-2 data, is also significantly negatively correlated with TSI (Figure 3b). Note that the two highest values of this index are recorded during the years 1987 and 2007 when TSI was extremely low. This suggests that the increase in frequency of RWP in this region during low TSI summers is a robust characteristic of TSI-RWP relationship.

While our primary focus is the relationship between extreme precipitation, flood frequency over western Europe, and TSI, we extended our analysis to examine extreme precipitation patterns associated with TSI on a global scale during the observational period. This expanded perspective aids in identifying potential mechanisms underlying the observed TSI forcing of floods in western Europe during the summer season. Consistent with the RWP frequency anomaly pattern (Figure 2), the frequency of extreme precipitation is higher in the region dominated by the positive RWP frequency anomalies in the Atlantic–European region during low total solar irradiance years (Figure 4). Strong anomalies of R90p indices are recorded in the tropical region, especially in the Pacific and Indian oceans. The R90p pattern shows large scale features as the global winter precipitation anomaly pattern

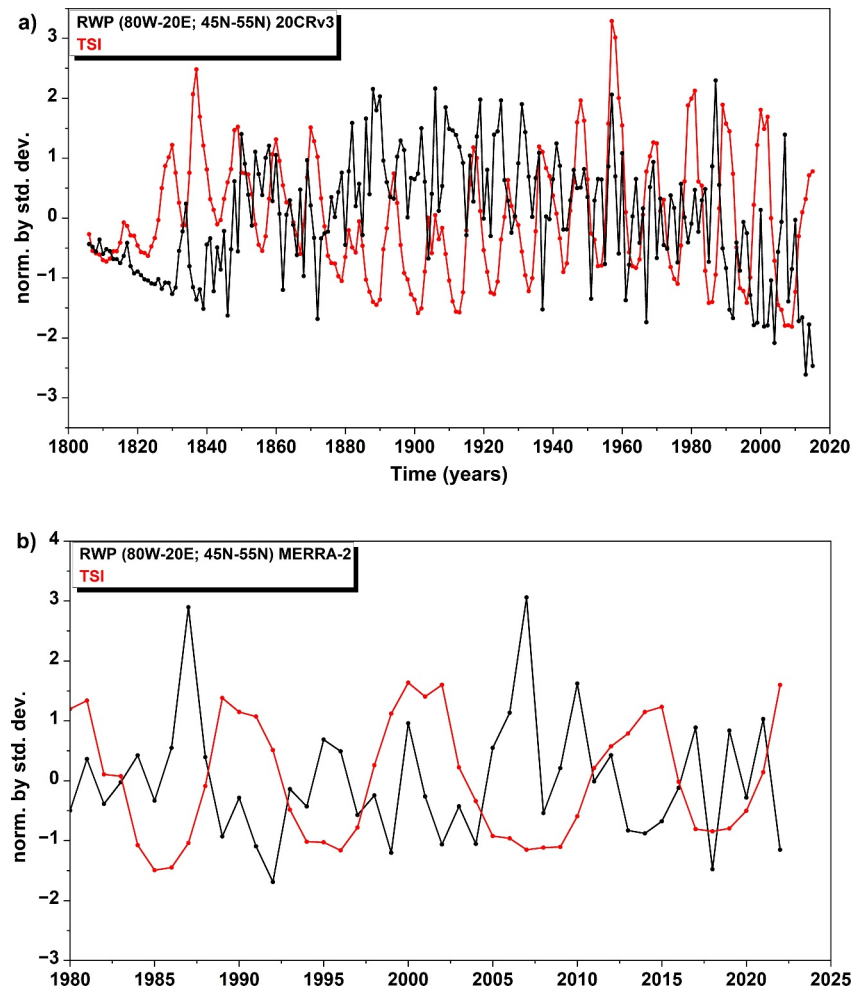


**Figure 3.** (a) Time series of the TSI (red) and an RWP index (black) for the period 1806–2015. The RWP index is defined as the average of RWP frequency, that is, percent of days with WPA >20 m/s, within the region (80°W–20°E; 45°N–55°N). The index is calculated using 20CRv3 data. (b) As in (a) but for the period 1980–2022 based on MERRA-2 data. Both time series are linear detrended and normalized with the corresponding standard deviation.

associated with high solar forcing as presented in previous studies (e.g., Gray et al., 2010 and references therein). However, it is possible that the low TSI signal is stronger recorded in R90p than in the precipitation mean field anomaly.

#### 4. RWP Patterns in Model Simulation

The RWP climatology corresponding the reference (REF1850) model simulation (Figure 5a) is consistent with previous RWP climatologies based on observations (e.g., Karami, 2019; Trevisiol et al., 2022). Similar patterns are recorded for grand solar minimum (GSM) experiment (Figure 5b). Both simulations captures well both the position and intensity of the North Atlantic, North Pacific, and Southern Hemisphere storm tracks. The difference between RWP frequency in GSM and REF1850 experiments (Figure 5c) shows a clear movement of the storm tracks toward the equator in both hemispheres. In the North Atlantic region, which is our focus, the pattern is similar to that in the observations (Figure 2), except in the Eastern Europe (Figure 5c). Consistent with our results, previous model simulations (e.g., Haigh, 1999) reveals a poleward shift of the mid-latitude storm tracks under high TSI forcing.

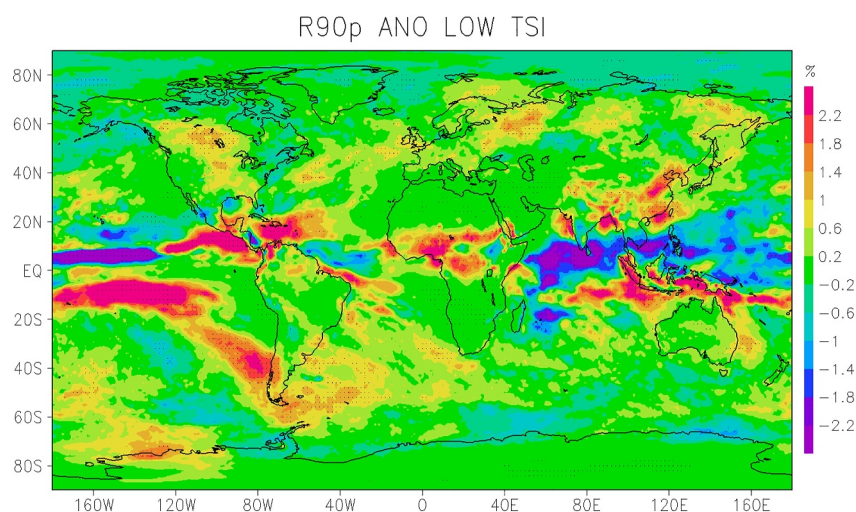


**Figure 4.** Composite map of extreme precipitation frequency anomalies during summer (see text for definition) for low total solar irradiance years during the 1806–2015 period. The dots mark cells with significant changes (90% confidence level). Units: %.

## 5. Paleoclimate Context

Paleoclimate reconstructions offer a critical window into Earth's past climate dynamics, extending far beyond the limited timeframe of instrumental records. By analyzing proxy data preserved in natural archives such as tree rings, ice cores, and sediments, scientists can reconstruct past temperature, precipitation, and atmospheric composition. These reconstructions provide crucial context for understanding the natural range of climate variability, allowing us to distinguish between natural fluctuations and human-induced climate change (Allen et al., 2022). In this respect, paleoclimate data can be used to test further the robustness of the atmospheric circulation patterns and associated precipitation extremes as derived from observed and model data in the current study.

First we look for the atmospheric circulation pattern associated with low TSI summers during the last four hundred years using paleo-reanalysis data. The analysis is performed for the period covered by both ModE-RA paleo-reanalysis data and TSI record, which is 1610–2008. The mean atmospheric circulation pattern anomaly associated with low TSI during this period (Figure 6) shows negative anomalies over entire tropical region, consistent with a general cooling of this region during low TSI summers. In the Atlantic–European region the anomaly pattern resembles the synoptic-scale pattern associated with river Ammer floods (Rimbu et al., 2016, 2021). A similar pattern is associated with the occurrence of debris flows in the Swiss Alps (Toreti et al., 2013). This suggests that the relationship between TSI forcing and synoptic-scale atmospheric circulation and associated extreme precipitation patterns over western Europe, as derived from observational data, are robust in the perspective of last four hundred years of climate variability.

To further investigate the persistence of the relationship between solar forcing, RWPs, and precipitation extremes over Europe across longer timescales, we examine the association between flood frequency, as documented in Ammersee sediments (Czymzik et al., 2013), and TSI extending back to 1610. Previous research studies (Rimbu et al., 2021) have demonstrated that the Ammersee sediment record serves as a reliable proxy for extreme precipitation frequency over western Europe during summer. Analysis of 10-year means, employed to enhance the signal-to-noise ratio, reveals a strong out-of-phase relationship between TSI and flood frequency at multidecadal timescales (Figure 7). A significant increase in flood frequency is recorded during both Maunder and Dalton solar minima (Figure 7), that is, around 1700's and 1820's, consistent with observational (Figure 2) and model (Figure 5c) RWP anomaly patterns. The flood and TSI time series are significantly negatively correlated ( $r = -0.41$ ,  $p < 0.1$ ) during the common period, that is 1610–1999. However, the flood record goes back in time to 3560 BC and the low frequency flood periods coincides well with low TSI periods (e.g., Rimbu et al., 2021). This suggests that flood and extreme precipitation patterns associated with TSI forcing, as described in previous sections, are independent of timescale.

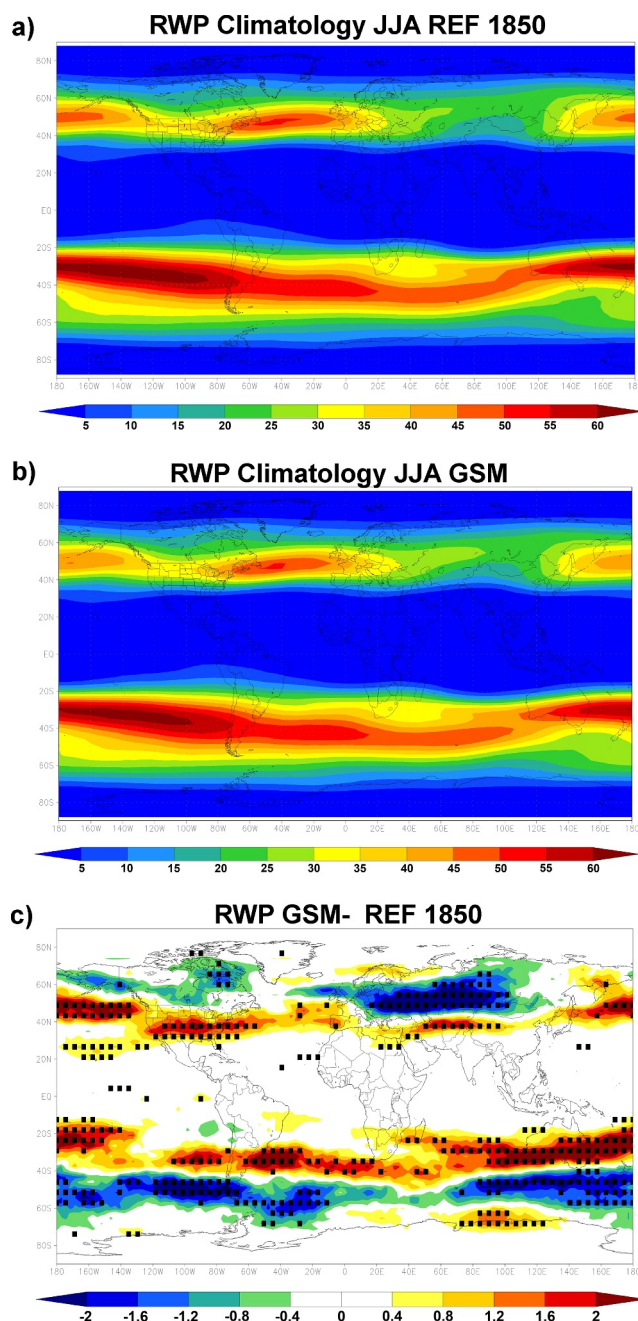


**Figure 5.** Climatology of RWP frequency, that is, WPA >20 m/s, for (a) reference (REF1850) and (b) grand solar minimum (GSM) experiment (c) difference between RWP frequency in GSM and REF1850 model simulation experiments. The dots mark cells with significant changes (90% confidence level). Units: %.

In a plausible scenario, a decrease in TSI in the next decades/centuries is expected (e.g., Matthes et al., 2017). The CMIP6 recommended TSI record (Matthes et al., 2017) shows a minimum in the second part of this century (Figure 7), which could be associated with an increase in the frequency of Sun-related extreme precipitation over western Europe relative to the present period.

## 6. Summary and Discussion

In this study, we have investigated the large-scale anomaly patterns in the frequency of RWPs and extreme precipitation over western Europe during boreal summer associated with the total solar irradiance variability. The

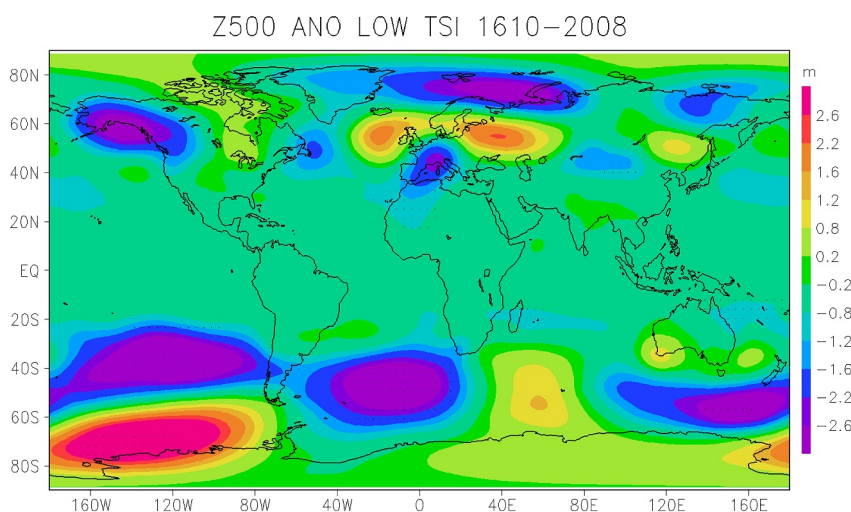


**Figure 6.** Composite map of 500 hPa geopotential height anomalies during summer associated with low TSI years during 1610–2008 period (see text for details). The dots mark cells with significant changes (90% confidence level). Units: m.

robustness of the results is addressed considering observed and proxy records as well as model data. We have shown that low TSI is associated with positive RWP frequency anomalies in the Atlantic–European region along  $\sim 50^\circ\text{N}$ . This corresponds to a southward displacement of the North Atlantic storm track relative to the climatology during low TSI summers. A similar relationship was identified in other reanalysis products, that is, MERRA-2 and NCEP, but for shorter periods. This suggests that the southward movement of the NA storm track during low TSI summers is a stable characteristic of solar impact on atmospheric circulation. This southward movement leads to positive anomalies of extreme precipitation and flood frequency over western Europe.

Previous modeling studies (e.g., Haigh, 1999) show a broadening of the tropical Hadley circulations and a poleward shifts of the storm tracks in both hemispheres for high TSI forcing. These model results suggest that the precise response of the atmosphere depends on the magnitude and distribution of the ozone changes in response to solar forcing. The model simulation analyzed here show similar patterns. However, additional analysis of our model data should be performed to identify the physical mechanism behind the solar related atmospheric circulation patterns, particularly the role of ozone change under solar irradiance forcing. Here we argue that the southern displacement of the storm track in the Atlantic–European region is associated with more frequent RWP and extreme precipitation over western Europe.

Furthermore, more frequent blocking should be recorded over eastern Europe during low TSI summers leading to more frequent extreme high temperature events over eastern Europe. However, more detailed model data analysis should be performed to assess the extreme temperature patterns associated with low TSI forcing.

Analysis of proxy data presented in this study indicates that the relationship between the TSI and the frequency of extreme summer rainfall is not dependent on timescale. With most scenarios/predictions (Matthes et al., 2017; Steinhilber & Beer, 2013) suggesting a decrease in TSI relative to the current maximum over the coming decades/centuries, we anticipate a gradual increase in solar-related extreme precipitation over western Europe, peaking in the second part of this century when a TSI minimum could be recorded. However, this is superimposed upon the anthropogenic forcing influencing RWP frequency. A recent model-based study (Trevisiol et al., 2022) suggests a decrease in RWP frequency in the North Atlantic region along  $\sim 50^\circ\text{N}$  during 2021–2040 and 2081–2100. This implies a poleward shift of the storm track and a consequent decrease in the frequency of extreme precipitation and floods over western Europe during these periods. Conversely, the TSI scenario considered here predicts a southward shift of the storm track with increased RWP and extreme precipitation frequency over

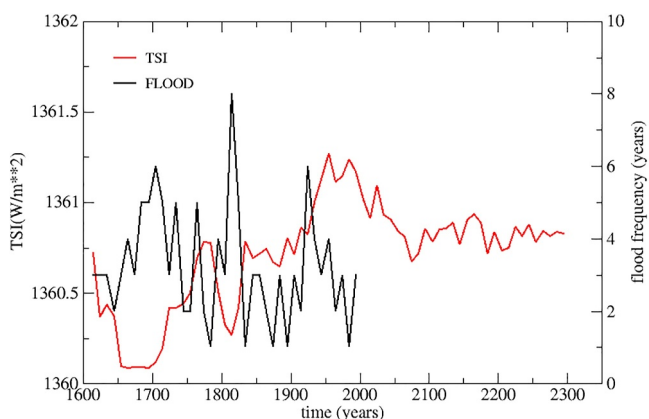


**Figure 7.** Time series of 10-year means of reconstructed total solar irradiance during the 1610–2300 (red) and flood frequency within 10-year bins recorded in Ammersee sediments (black) during the 1610–1999 periods (see text for details). Units:  $\text{W}/\text{m}^2$  and number of flood years recorded in a 10-year bin.

western Europe. Based on these findings and model simulations (Trevisiol et al., 2022 and references therein), we infer that TSI forcing on RWP frequency in the North Atlantic is weaker than anthropogenic forcing over the next decades/centuries. However, paleoclimate data suggest that TSI is the dominant forcing on flood and extreme precipitation events over western Europe at longer timescales (centennial to millennial) during the past five millennia (e.g., Rimbu et al., 2021).

To conclude, we have identified RWP frequency anomaly patterns and associated extreme precipitation events over western Europe during boreal summer, linked to low total solar irradiance forcing. The robustness of these patterns has been demonstrated across diverse observational and reconstructed data sets. However, further modeling experiments are necessary to elucidate the precise mechanisms underlying the relationship between solar irradiance forcing and extreme weather and climate phenomena observed in our analysis. Expanding upon the findings presented here, our analytical approach could be applied to identify RWP frequency anomaly patterns associated with solar irradiance forcing in other seasons, when RWP activity is typically higher than during summer (e.g., Karami, 2019). This would enhance our understanding of the relative contributions of natural (solar irradiance) and anthropogenic forcing to extreme weather and climate variability.

### Data Availability Statement

All data sets used in this study are available from public repositories. The TSI data for the period 1610–1849 (Coddington et al., 2017) is available at <https://doi.org/10.7289/V56W985W>. The TSI data for the period 1850–2299 (Matthes et al., 2017) is available through Geomar Data Store site (<https://solarisheppa.geomar.de/cmip6>). The reanalysis data, that is, 20CRv3 (Slivinsky et al., 2019) and NCEP (Kalnay et al., 1996) are available through the PSL/NOAA Data Store (<https://www.psl.noaa.gov/data/gridded/>). The MERRA-2 reanalysis (Gelaro et al., 2017) is available through Global Modeling and Assimilation Office (GMAO) (<https://gmao.gsfc.nasa.gov/reanalysis/MERRA-2/>). The model data (T. Spiegl et al., 2023) is available through SLOCHECK Project Data Store ([https://www.wdc-climate.de/ui/entry?acronym=DKRZ\\_LTA\\_519\\_ds00048](https://www.wdc-climate.de/ui/entry?acronym=DKRZ_LTA_519_ds00048)). The Ammersee flood record (Czymzik et al., 2012) is available via PANGAEA database <https://doi.org/10.1594/PANGAEA.803368>. The ModE-RA paleo-reanalysis data (Valler et al., 2023) is available at [https://doi.org/10.26050/WDCC/ModE-RA\\_s14203-18501](https://doi.org/10.26050/WDCC/ModE-RA_s14203-18501).

### References

- Allen, K. J., Reide, F., Gouramanis, C., Keenan, B., Stoffel, M., Hu, A., & Ionita, M. (2022). Coupled insights from the palaeoenvironmental, historical and archaeological archives to support social-ecological resilience and the sustainable development goals. *Environmental Research Letters*, 17(5), 055011. <https://doi.org/10.1088/1748-9326/ac6967>
- Altenhoff, A. M., Martius, O., Croci-Maspoli, M., Schwierz, C., & Davies, H. C. (2008). Linkage of atmospheric blocks and synoptic-scale Rossby waves: A climatological analysis. *Tellus*, 60(5), 1053–1063. <https://doi.org/10.1111/j.1600-0870.2008.00354.x>
- Büntgen, U., Tegel, W., Nicolussi, K., McCormick, M., Frank, D., Trouet, V., et al. (2011). 2500 years of European climate variability and human susceptibility. *Science*, 331(6017), 578–582. <https://doi.org/10.1126/science.1197175>
- Camenisch, C., Keller, K. M., Salvisberg, M., Amann, B., Bauch, M., Blumer, S., et al. (2016). The 1430s: A cold period of extraordinary internal climate variability during the early Spörer Minimum with social and economic impacts in north-western and central Europe. *Climate of the Past*, 12, 2107–2126. <https://doi.org/10.5194/cp-12-2107-2016>
- Campitelli, E. (2021). metR: Tools for easier analysis of meteorological fields [Software]. *R package version v0.14.0*. <https://doi.org/10.5281/zenodo.2593516>
- Chiodo, G., Oehrlein, J., Polvani, L. M., Fyfe, J. C., & Smith, A. K. (2019). Insignificant influence of the 11-year solar cycle on the North Atlantic oscillation. *Nature Geoscience*, 12, 94–99. <https://doi.org/10.1038/s41561-018-0293-3>
- Coddington, O., Lean, J. L., Lindholm, D., Pilewskie, P., Snow, M., & NOAA CDR Program. (2017). NOAA climate data record (CDR) of total solar irradiance (TSI), NRLTSI version 2.1 [Dataset]. NOAA National Centers for Environmental Information. <https://doi.org/10.7289/V56W985W>
- Czymzik, M., Brauer, A., Dulski, P., Plessen, B., Naumann, R., von Grafenstein, U., & Scheffler, R. (2012). Flood layer data from Ammersee sediment profile AS10prox [Dataset]. PANGAEA. <https://doi.org/10.1594/PANGAEA.803368>
- Czymzik, M., Brauer, A., Dulski, P., Plessen, B., von Grafenstein, U., Naumann, R., & Scheffler, R. (2013). Orbital and solar forcing of shifts in mid-to late Holocene flood intensity from varved sediments of pre-alpine Lake Ammersee (southern Germany). *Quaternary Science Reviews*, 61, 96–110. <https://doi.org/10.1016/j.quascirev.2012.11.010>
- Czymzik, M., Muscheler, R., & Brauer, A. (2016). Solar modulation of flood frequency in central Europe during spring and summer on inter-annual to multi-centennial timescales. *Climate of the Past*, 12(3), 799–805. <https://doi.org/10.5194/cp-12-799-2016>
- de Vries, A. J. (2021). A global climatological perspective on the importance of Rossby wave breaking and intense moisture transport for extreme precipitation events. *Weather and Climate Dynamics*, 2(1), 129–161. <https://doi.org/10.5194/wcd-2-129-2021>
- Egorova, T., Schmutz, W., Rozanov, E., Shapiro, A. I., Usoskin, I., Beer, J., et al. (2018). Revised historical solar irradiance forcing. *Astronomy and Astrophysics*, 615, A85. <https://doi.org/10.1051/0004-6361/201731199>
- Fragkoulidis, G. (2022). Decadal variability and trends in extratropical Rossby wave packet amplitude, phase, and phase speed. *Weather and Climate Dynamics*, 3(4), 1381–1398. <https://doi.org/10.5194/wcd-3.1381-2022>
- Funke, B., Dudok de Wit, T., Ermolli, I., Haberleiter, M., Kinnison, D., Marsh, D., et al. (2024). Towards the definition of a solar forcing dataset for CMIP7. *Geoscientific Model Development*, 17(3), 1217–1227. <https://doi.org/10.5194/gmd-17-1217-2024>

### Acknowledgments

N. R., T. S., M. I. and G. L are supported by Helmholtz Association through the joint program “Changing Earth - Sustaining our Future” (PoF IV) of the AWI. This work was supported by funding from the Federal Ministry of Education and Research (BMBF) and the Helmholtz Research Field Earth and Environment for the Innovation Pool Project SCENIC and from the Helmholtz Climate Initiative REKLIM. S. D. was funded by the AWI Inspires Project - “Compound extreme events: a long-term perspective (LongCEX).” The analyzed chemistry-climate model data have been provided by the BMBF funded project “Solar contribution to climate change on decadal to centennial timescales (SOLCHECK).” We would like to thank the anonymous reviewers for their suggestions and comments that lead to a significant improvement of the manuscript.

- Gelaro, R., McCarty, W., Suárez, M. J., Todling, R., Molod, A., Takacs, L., et al. (2017). The modern Eran retrospective analysis for research and Applications, version 2 (MERRA-2). *Journal of Climate*, 30(14), 5419–5454. <https://doi.org/10.1175/JCLI-D-16-0758.1>
- Gray, L. J., Beer, J., Geller, M., Haigh, J. D., Lockwood, M., Matthes, K., et al. (2010). Solar influences on climate. *Reviews of Geophysics*, 48(4). <https://doi.org/10.1029/2009RG000282>
- Haigh, J. D. (1999). A GCM study of climate change in response to the 11-year solar cycle. *Quarterly Journal of Meteorological Society*, 125(555), 871–892. <https://doi.org/10.1002/qj.49712555506>
- Jöckel, P., Tost, H., Pozzer, A., Kunze, M., Kirner, O., Brenninkmeijer, C. A., et al. (2016). Earth system chemistry integrated modelling (ESCI-Mo) with the modular earth submodel system (MESSy) version 2.51. *Geoscientific Model Development*, 9(3), 1153–1200. <https://doi.org/10.5194/gmd-9-1153-2016>
- Jones, P. D., & Mann, M. E. (2004). Climate over past millennia. *Review of Geophysics*, 42(2), RG2002. <https://doi.org/10.1029/2003RG000143>
- Jungclaus, J. H., Keenlyside, N., Botzet, M., Haak, H., Luo, J.-J., Latif, M., et al. (2006). Ocean circulation and tropical variability in the coupled model ECHAM5/MPI-OM. *Journal of Climate*, 19(16), 3952–3972. <https://doi.org/10.1175/JCLI3827.1>
- Kalnay, E., Kanamitsu, M., Kistler, R., Collins, W., Deaven, D., Gandin, L., et al. (1996). The NCEP/NCAR 40-year reanalysis project. *Bulletin of the American Meteorological Society*, 77(3), 437–472. [https://doi.org/10.1175/1520-0477\(1996\)077<0437:TNYRP>2.0.CO;2](https://doi.org/10.1175/1520-0477(1996)077<0437:TNYRP>2.0.CO;2)
- Karami, K. (2019). Upper tropospheric Rossby wave packets: Long-term trends and variability. *Theoretical and Applied Climatology*, 138, 527–540. <https://doi.org/10.1007/s00704-019-02845-5>
- Kodera, K., & Kuroda, Y. (2002). Dynamical response to the solar cycle. *Journal of Geophysical Research*, 107(D24), ACL 5-1–ACL 5-12. <https://doi.org/10.1029/2002JD002224>
- Kunze, M., Godolt, M., Langematz, U., Grenfell, J. L., Hamann-Reinus, A., & Rauer, H. (2014). Investigating the early Earth faint young Sun problem with a general circulation model. *Planetary and Space Science*, 98, 77–92. <https://doi.org/10.1016/j.pss.2013.09.011>
- Lohmann, G., Rambu, N., & Dima, M. (2004). Climate signature of solar irradiance variations: Analysis of long-term instrumental, historical, and proxy data. *International Journal of Climatology*, 24(8), 1045–1056. <https://doi.org/10.1002/joc.1054>
- Luterbacher, J., Rickli, R., Xoplaki, E., Tinguely, C., Beck, C., Pfister, C., & Wanner, H. (2001). The late Maunder minimum (1675–1715)—a key period for studying decadal scale climatic change in Europe. *Climatic Change*, 49(4), 441–462. <https://doi.org/10.1023/A:1010667524422>
- Matthes, K., Funke, B., Andersson, M. E., Barnard, L., Beer, J., Charbonneau, P., et al. (2017). Solar forcing for CMIP6 (v3.2). *Geoscientific Model Development*, 10(6), 2247–2302. <https://doi.org/10.5194/gmd-10-2247-2017>
- Nissen, K. M., Matthes, K., Langematz, U., & Mayer, B. (2007). Towards a better representation of the solar cycle in general circulation models. *Atmospheric Chemistry and Physics*, 7(20), 5391–5400. <https://doi.org/10.5194/acp-7-5391-2007>
- Pérez, I., Barreiro, M., & Masoller, C. (2021). ENSO and SAM influence on the generation of long episodes of Rossby wave packets during southern hemisphere summer. *Journal of Geophysical Research: Atmospheres*, 126(24), e2021JD035467. <https://doi.org/10.1029/2021JD035467>
- Quinting, J. F., & Vitart, F. (2019). Representation of synoptic-scale Rossby waves packets and blocking in the S2S prediction project database. *Geophysical Research Letters*, 46(2), 1070–1078. <https://doi.org/10.1029/2018GL081381>
- Rimbu, N., Czymzik, M., Ionita, M., Lohmann, G., & Brauer, A. (2016). Atmospheric circulation patterns associated with the variability of River Ammer floods: Evidence from observed and proxy data. *Climate of the Past*, 12(2), 377–385. <https://doi.org/10.5194/cp-12-377-2016>
- Rimbu, N., Lohmann, G., Ionita, M., Czymzik, M., & Brauer, A. (2021). Interannual to millennial-scale variability of River Ammer floods and its relationship with solar forcing. *International Journal of Climatology*, 41(S1), E644–E655. <https://doi.org/10.1002/joc.6715>
- Riviere, G., & Orlansky, I. (2007). Characteristics of the Atlantic storm-track Eddy activity and its relation with the North Atlantic oscillation. *Journal of Atmospheric Sciences*, 64(2), 241–266. <https://doi.org/10.1175/JAS3850.1>
- Roeckner, E., Brokopf, R., Esch, M., Giorgetta, M., Hagemann, S., Kornblüeh, L., et al. (2006). Sensitivity of simulated climate to horizontal and vertical resolution in the ECHAM5 atmosphere model. *Journal of Climate*, 19(16), 3771–3791. <https://doi.org/10.1175/JCLI3824.1>
- Roy, I. (2018). Climate variability and sunspot activity. ISSN 2194-5217. ISBN 978-3-319-77106-9. In *Analysis of the Solar Influence on Climate*. Springer Atmospheric Sciences. <https://doi.org/10.1007/978-3-319-77107-6>
- Sander, R., Kerkweg, A., Jöckel, P., & Lelieveld, J. (2005). The new comprehensive atmospheric chemistry module MECCA. *Atmospheric Chemistry and Physics*, 5(2), 445–450. <https://doi.org/10.5194/acp-5-445-2005>
- Slivinski, L. C., Compo, G. P., Whitaker, J. S., Sardesemukh, P. D., Giese, B. S., McColl, C., et al. (2019). Towards a more reliable historical reanalysis: Improvements for version 3 of 6 the twentieth century reanalysis system. *Quarterly Journal of Royal Meteorological Society*, 145(724), 2876–2908. <https://doi.org/10.1002/qj.3598>
- Souders, M. B., Colle, B. A., & Chang, E. K. M. (2014). The climatology and characteristics of Rossby Wave Packets using featured based tracking techniques. *Monthly Weather Review*, 142(10), 3258–3548. <https://doi.org/10.1175/MWR-D-13-00371.1>
- Spiegel, T., & Langematz, U. (2020). Twenty-first-century climate change hot spots. *Journal of Climate*, 33(9), 3431–3447. <https://doi.org/10.1175/JCLI-D-19-0059.1>
- Spiegel, T., Wahl, S., Huo, W., Schmidt, F., & Langematz, U. (2023). ROMIC-II-SOLCHECK joint database part II - Grand Solar Minimum sensitivity experiments under different climatic background [Dataset]. *DOKU at DKRZ*. [https://www.wdc-climate.de/ui/entry?acronym=DKRZ\\_LTA\\_519\\_ds00048](https://www.wdc-climate.de/ui/entry?acronym=DKRZ_LTA_519_ds00048)
- Spiegel, T. C., Langematz, U., Pohlmann, H., & Kröger, J. (2023). A critical evaluation of decadal solar cycle imprints in the MiKlip historical ensemble simulations. *Weather and Climate Dynamics*, 4(3), 789–807. <https://doi.org/10.5194/wcd-4-789-2023>
- Steinhilber, F., & Beer, J. (2013). Prediction of solar activity for the next 500 years. *Journal of Geophysical Research*, 118(5), 1861–1867. <https://doi.org/10.1002/jgra.50210>
- Strong, C., & Magnusdottir, G. (2008). Tropospheric Rossby wave breaking and the NAO/NAM. *Journal of Atmospheric Sciences*, 65(9), 2861–2876. <https://doi.org/10.1175/2008JAS2632.1>
- Toreti, A., Schneuwly-Bollschweiler, M., Stoffel, M., & Luterbacher, J. (2013). Atmospheric forcing of debris flows in the southern Swiss Alps. *Journal of Applied Meteorology and Climatology*, 52(7), 1554–1560. <https://doi.org/10.1175/JAMC-D-13-077.1>
- Trevisiol, A., Gili, L., & Faggian, P. (2022). Short and long-term projections of Rossby wave packets and blocking events with particular attention to the northern hemisphere. *Global and Planetary Change*, 209, 103750. <https://doi.org/10.1016/j.gloplacha.2022.103750>
- Valler, V., Franke, J., Brugnara, Y., Burgdorf, A. M., Lundstad, E., Hand, R., et al. (2023). ModE-RA - a global monthly paleo-reanalysis of the modern era (1421 to 2008): Set 1420-3\_1850-1 [Dataset]. *World Data Center for Climate (WDCC) at DKRZ*. [https://doi.org/10.26050/WDCC/ModE-RA\\_s14203-18501](https://doi.org/10.26050/WDCC/ModE-RA_s14203-18501)
- Valler, V., Franke, J., Brugnara, Y., Samakinwa, E., Hand, R., Lundstad, E., et al. (2024). ModE-RA: A global monthly paleo-reanalysis of the modern era 1421 to 2008. *Scientific Data*, 11(1), 36. <https://doi.org/10.1038/s41597-023-02733-8>
- von Storch, H., & Zwiers, F. (1999). *Statistical analysis in climate research*. Cambridge University Press. <https://doi.org/10.1017/CBO9780511612336>

- Wirth, V., Riemer, M., Chang, E. K. M., & Martius, O. (2018). Rossby wave packets on the midlatitude waveguide-A review. *Monthly Weather Review*, *146*(7), 1965–2001. <https://doi.org/10.1175/MWR-D-16-0483.1>
- Zhang, X., Alexander, L., Hegerl, G. C., Jones, P., Klein Tank, A., Peterson, T. C., et al. (2011). Indices for monitoring changes in extremes based on daily temperature and precipitation data. *WIREs Climate Change*, *2*(6), 851–870. <https://doi.org/10.1002/wcc.147>
- Zimin, A. V., Sznuyogh, I., Patil, D. J., Hunt, B. R., & Ott, E. (2003). Extracting envelopes of Rossby wave packets. *Monthly Weather Review*, *131*(5), 1011–1017. [https://doi.org/10.1175/1520-0493\(2003\)131<1011:EEORWP>2.0.CO;2](https://doi.org/10.1175/1520-0493(2003)131<1011:EEORWP>2.0.CO;2)